Granular contact dynamics using mathematical programming methods

K. Krabbenhoft [a,b,*], A.V. Lyamin [a], J. Huang [a], M. Vicente da Silva [a,c]

[a] Centre for Geotechnical Science and Engineering, University of Newcastle, NSW, Australia
[b] Department of Industrial and Civil Engineering, University of Southern Denmark, Odense, Denmark
[c] Departamento de Engenharia Civil, Universidade Nova de Lisboa, Portugal

ARTICLE INFO

ABSTRACT

A class of variational formulations for discrete element analysis of granular media is presented. These formulations lead naturally to convex mathematical programs that can be solved using standard and readily available tools. In contrast to traditional discrete element analysis, the present granular contact dynamics formulation uses an implicit time discretization, thus allowing for large time steps. Moreover, in the limit of an infinite time step, the general dynamic formulation reduces to a static formulation that is useful in simulating common quasi-static problems such as triaxial tests and similar laboratory experiments. A significant portion of the paper is dedicated to exploring the consequences of the associated frictional sliding rule implied by the variational formulation adopted. In this connection, a new interior-point algorithm for general linear complementarity problems is developed and it is concluded that the associated sliding rule, in the context of granular contact dynamics, may be viewed as an artifact of the time discretization and that the use of an associated flow rule at the particle scale level generally is physically acceptable.

© 2012 Elsevier Ltd. All rights reserved.

1. Introduction

Since being introduced in the 1970s [15], the Discrete Element Method (DEM) has become a standard tool in geomechanics and related fields. The basic idea behind the method is to consider an assembly of grains each governed by Newton's laws of motion. Interaction between grains is accounted for by relating the overlap that may occur between grains to forces via an appropriate constitutive relation. This is typically done in an explicit manner where the positions of the particles are first advanced by a suitably small time increment after which the contact forces are calculated on the basis of the particle overlaps. The combination of an explicit contact force calculation and usually rather stiff particles necessitates the use of very small time increments and thus potentially a large overall computational time.

An alternative to the classical DEM is contained in the so-called Non-Smooth Contact Dynamics Method developed by Moreau, Jean and their coworkers [21,42]. Particle interaction is here accounted for in an implicit manner. In contrast to the classical DEM, the particles are considered perfectly rigid and contact forces are those that imply non-penetration of the particles. Also, since the time discretization is implicit, large time steps can be used, with the exact interaction effectively being averaged over the time step. Although the classical DEM has been much more widely applied to granular media than the contact dynamics approach, a number of studies have been conducted using the latter method and have generally shown a favorable performance [20,31,40,44,48–52,57,58,62].

The primary reason for the relatively scarce application of the contact dynamics method to granular media is probably that it is perceived to be much more complex to implement than the classical DEM [16]. Notwithstanding the validity of this perception, it is definitely true that there are fewer concise 'recipes' for contact dynamics than for the classical DEM. Moreover, while the classical DEM leaves little room for variation, there are numerous contact dynamics algorithms that each display significant variation between one another (see for example [1,21,46,60]).

In this paper, a variational approach to contact dynamics is presented. From a numerical point of view, the approach leads naturally to a formulation in terms of mathematical programming. The resulting programs can be solved using standard and readily available algorithms. In terms of implementation, the key operations comprise the assembly of system matrices similar to those of the finite element method. These system matrices define the mathematical program to be solved in each time step. The final, and crucial, task of solving these programs can be carried out using a general purpose solver – in 2D a quadratic programming solver and in 3D a second-order cone programming solver. Such solvers are becoming increasingly common and both commercial and open-source codes are readily available [6,7]. In this paper we use both a quadratic programming algorithm of the interior-point type which is detailed in Section 4 as well as a second-order cone programming solver, SONIC, that we have previously developed

* Corresponding author at: Centre for Geotechnical Science and Engineering, University of Newcastle, NSW, Australia.

E-mail address: kristian.krabbenhoft@newcastle.edu.au (K. Krabbenhoft).

with computational plasticity applications in mind [25]. As such, with appropriate solvers being readily available, the implementation is in fact very simple and, in our opinion, considerably less complex than that of the classical DEM.

The paper is organized as follows. In Section 2, the basic frictionless contact problem is considered and various possible mathematical programming formulations are discussed. Frictional contact is then introduced in Section 3. We here emphasize the consequences of the associated frictional sliding rule implied by the variational formulation adopted. In particular, we show that the undesirable dilation implied by the associated sliding rule can be interpreted as an artifact of the time discretization. This rather remarkable fact suggests that a standard associated formulation in fact is suitable, contrary to what might be expected. Nevertheless, in Section 4 we consider a fully nonassociated formulation and develop an algorithm for the resulting linear complementarity problem. This algorithm further serves to validate the postulate that the effects of dilation for problems of practical interest are negligible, even for large time steps. This is demonstrated by application to a number of common benchmark problems in Section 5 before conclusions are drawn in Section 6.

Matrix notation is used throughout with bold upper and lower case letters representing matrices and vectors respectively and with $^\top$ denoting the transpose.

2. Frictionless contact

2.1. Equations of motion

The equations of motion for a single frictionless particle are given by

$$m\dot{\boldsymbol{v}}(t) = \boldsymbol{f}_{\text{ext}} \tag{1}$$

where $\boldsymbol{v}(t) = (v_x(t), v_y(t))^\top$ are the linear velocities, m is the mass, and $\boldsymbol{f}_{\text{ext}} = (f_x, f_y)_{\text{ext}}^\top$ are external forces.

2.1.1. Time discretization

Relating position to velocity by $\dot{\boldsymbol{x}}(t) = \boldsymbol{v}(t)$, the equations of motion can be written as

$$m\dot{\boldsymbol{v}}(t) = \boldsymbol{f}_{\text{ext}}$$
$$\boldsymbol{v}(t) = \dot{\boldsymbol{x}}(t) \tag{2}$$

These equations are discretized by the θ-method:

$$m\frac{\boldsymbol{v} - \boldsymbol{v}_0}{\Delta t} = \boldsymbol{f}_{\text{ext}}$$
$$\theta\boldsymbol{v} + (1-\theta)\boldsymbol{v}_0 = \frac{\boldsymbol{x} - \boldsymbol{x}_0}{\Delta t} \tag{3}$$

where $0 \leqslant \theta \leqslant 1$ and $\boldsymbol{x}_0$ and $\boldsymbol{v}_0$ are the known position and velocity at time t_0 while $\boldsymbol{x}$ and $\boldsymbol{v}$ are the corresponding quantities at time $t_0 + \Delta t$. Straightforward manipulations lead to the following expressions for the displacements and velocities at time $t_0 + \Delta t$:

$$\bar{m}\Delta\boldsymbol{x} = \bar{\boldsymbol{f}}_0$$
$$\boldsymbol{v} = \frac{1}{\theta}\left[\frac{\Delta\boldsymbol{x}}{\Delta t} - (1-\theta)\boldsymbol{v}_0\right] \tag{4}$$

where

$$\bar{m} = \frac{1}{\theta\Delta t^2}m, \quad \bar{\boldsymbol{f}}_0 = \boldsymbol{f}_{\text{ext}} + \bar{m}\boldsymbol{v}_0\Delta t \tag{5}$$

and $\Delta\boldsymbol{x} = \boldsymbol{x} - \boldsymbol{x}_0$ are the displacements. The stability properties of the θ-method are well known: for $\theta = \frac{1}{2}$ the unconditionally stable and energy preserving Newmark average acceleration scheme is recovered, for $\theta > \frac{1}{2}$ the scheme is unconditionally stable and dissipative, and for $\theta < \frac{1}{2}$ stability depends on the time step. In the context of collisions, the algorithmic energy dissipation that occurs
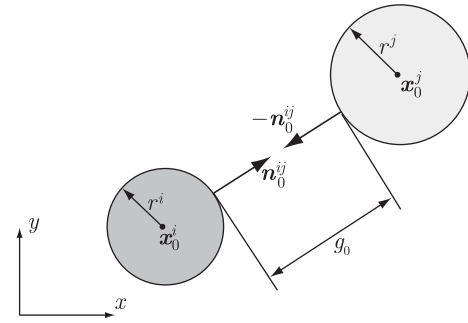

Fig. 1. Frictionless contact geometry.

for $\theta > \frac{1}{2}$ can be related to the physical dissipation associated with impact and thus to the restitution coefficient. Indeed, as will be shown in Section 2.7, a value of $\theta = \frac{1}{2}$ corresponds to an elastic collision while $\theta = 1$ reproduces a perfectly inelastic collision.

2.2. Non-penetration condition

Consider two circular particles as shown in Fig. 1. The positions of the particles at time t_0 are given by $\boldsymbol{x}_0^i$ and $\boldsymbol{x}_0^j$. The condition that the particles do not penetrate each other at time $t_0 + \Delta t$ can be stated as

$$\|\boldsymbol{x}^i - \boldsymbol{x}^j\| \geqslant r^i + r^j \tag{6}$$

This inequality constraint is non-convex for spatial dimensions greater than one and thus problematic to deal with using standard mathematical programming methods. Consequently, throughout this paper, we consider the linear approximation:

$$\left(\boldsymbol{n}_0^{ij}\right)^\top(\Delta\boldsymbol{x}^i - \Delta\boldsymbol{x}^j) - g_0 \leqslant 0 \tag{7}$$

where

$$\boldsymbol{n}_0^{ij} = \frac{\boldsymbol{x}_0^j - \boldsymbol{x}_0^i}{\|\boldsymbol{x}_0^i - \boldsymbol{x}_0^j\|}, \quad g_0 = \|\boldsymbol{x}_0^i - \boldsymbol{x}_0^j\| - (r^i + r^j) \tag{8}$$

are the initial normal and gap respectively (see Fig. 1).

2.3. Governing equations

We now consider the problem of frictionless contact involving two particles, i and j. In this case the governing equations comprise momentum balance for each particle (incorporating contact forces), the linearized non-penetration condition and conditions ensuring that the contact forces are positive only if the gap is closed and otherwise zero. These requirements can be stated in terms of the following time discrete governing equations:

$$\bar{m}^i\Delta\boldsymbol{x}^i = \bar{\boldsymbol{f}}_0^i - \boldsymbol{n}_0^{ij}p$$
$$\bar{m}^j\Delta\boldsymbol{x}^j = \bar{\boldsymbol{f}}_0^j + \boldsymbol{n}_0^{ij}p$$
$$\left(\boldsymbol{n}_0^{ij}\right)^\top(\Delta\boldsymbol{x}^i - \Delta\boldsymbol{x}^j) - g_0 \leqslant 0 \tag{9}$$
$$p \geqslant 0$$
$$p\left[\left(\boldsymbol{n}_0^{ij}\right)^\top(\Delta\boldsymbol{x}^i - \Delta\boldsymbol{x}^j) - g_0\right] = 0$$

where p is the contact force. These equations may be solved by trial and error. Assume first that $p = 0$ and solve the equations of motion to compute the displacements, $\Delta\boldsymbol{x}^i$ and $\Delta\boldsymbol{x}^j$. If these are such that penetration occurs, p is considered an unknown and the equations of motion are solved with the additional condition that $\left(\boldsymbol{n}_0^{ij}\right)^\top(\Delta\boldsymbol{x}^i - \Delta\boldsymbol{x}^j) - g_0 = 0$. This procedure is very similar to the fully

implicit stress integration, or closest-point projection, scheme used in computational plasticity [53,56] and the governing Eq. (9) do indeed define a similar closest-point projection problem as will be discussed next.

2.4. Variational formulation

Before proceeding with a variational formulation of the governing Eq. (9), it is convenient to introduce the following matrix quantities which cover general n-particle systems:

$$\begin{aligned}
&\overline{\boldsymbol{M}} = \text{diag}(\bar{m}^1, \bar{m}^1, \ldots, \bar{m}^n, \bar{m}^n) \\
&\boldsymbol{x} = (\boldsymbol{x}^1, \ldots, \boldsymbol{x}^n), \boldsymbol{v} = (\boldsymbol{v}^1, \ldots, \boldsymbol{v}^n) \\
&\boldsymbol{g} = (g^1, \ldots, g^N), \boldsymbol{p} = (p^1, \ldots, p^N)
\end{aligned} \tag{10}$$

where n is the number of particles and N is the number of contacts. Furthermore, collecting the normals associated with potential contacts in a matrix $\boldsymbol{N}$, the governing Eq. (9) can be written as:

$$\begin{aligned}
&\overline{\boldsymbol{M}}\Delta\boldsymbol{x} + \boldsymbol{N}_0\boldsymbol{p} = \bar{\boldsymbol{f}}_0 \\
&\boldsymbol{N}_0^\top\Delta\boldsymbol{x} - \boldsymbol{g}_0 \leqslant \boldsymbol{0} \\
&\boldsymbol{p} \geqslant \boldsymbol{0} \\
&\boldsymbol{P}(\boldsymbol{N}_0^\top\Delta\boldsymbol{x} - \boldsymbol{g}_0) = \boldsymbol{0}
\end{aligned} \tag{11}$$

where $\boldsymbol{P} = \text{diag}(\boldsymbol{p})$ and subscripts 0 again refer to the known state. These equations constitute the first-order Karush–Kuhn–Tucker (KKT) optimality conditions associated with the following optimization problem, or variational principle:

$$\min_{\boldsymbol{x}} \max_{\boldsymbol{p}} \quad \{\tfrac{1}{2}\Delta\boldsymbol{x}^\top\overline{\boldsymbol{M}}\Delta\boldsymbol{x} - \Delta\boldsymbol{x}^\top\bar{\boldsymbol{f}}_0\} + \{\Delta\boldsymbol{x}^\top\boldsymbol{N}_0\boldsymbol{p} - \boldsymbol{g}_0^\top\boldsymbol{p}\} \\ \text{subject to} \quad \boldsymbol{p} \geqslant \boldsymbol{0} \tag{12}$$

The first term in the objective function is a time discrete form of the action integral associated with a collection of non-interacting particles while the second term accounts for the effects of contact. This principle reproduces the governing equation (11) after which the velocities at time $t_1 = t_0 + \Delta t$ are calculated from (4) and used to set up a new optimization problem to determine the displacements at time t_2, etc.

2.5. Displacement based problem

The variational principle (12) can alternatively be cast in terms of a problem involving only displacements:

$$\begin{aligned}
&\text{minimize} \quad \tfrac{1}{2}\Delta\boldsymbol{x}^\top\overline{\boldsymbol{M}}\Delta\boldsymbol{x} - \Delta\boldsymbol{x}^\top\bar{\boldsymbol{f}}_0 \\
&\text{subject to} \quad \boldsymbol{N}_0^\top\Delta\boldsymbol{x} - \boldsymbol{g}_0 \leqslant \boldsymbol{0}
\end{aligned} \tag{13}$$

The contact forces are here recovered as part of the solution, namely as the Lagrange multipliers associated with the inequality constraints (see Appendix A for details).

2.6. Force based problem

Finally, it may be shown that (12) and (13) are equivalent to the following problem involving only forces:

$$\begin{aligned}
&\text{maximize} \quad -\tfrac{1}{2}\boldsymbol{r}^\top\overline{\boldsymbol{M}}^{-1}\boldsymbol{r} - \boldsymbol{g}_0^\top\boldsymbol{p} \\
&\text{subject to} \quad \boldsymbol{r} + \boldsymbol{N}_0\boldsymbol{p} = \bar{\boldsymbol{f}}_0 \\
&\qquad\qquad\quad \boldsymbol{p} \geqslant \boldsymbol{0}
\end{aligned} \tag{14}$$

where $\boldsymbol{r}$ are to be interpreted as dynamic forces. The displacements are here recovered as the Lagrange multipliers associated with the equality constraints.

In summary, the governing equation (11) can be cast in terms of three different but equivalent variational statements: the mixed force–displacement problem (12), the displacement based problem (13), and the force based problem (14). Each of these three problems have their merits in terms of providing physical insights and forming the basis for computations.

2.7. Restitution coefficient

Consider two particles not subjected to any external forces. From (9) we have

$$\begin{aligned}
&m^i \boldsymbol{v}^i = \theta\Delta t^2 \boldsymbol{n}_0^{ij} p + m^i \boldsymbol{v}_0^i \\
&m^j \boldsymbol{v}^j = -\theta\Delta t^2 \boldsymbol{n}_0^{ij} p + m^j \boldsymbol{v}_0^j
\end{aligned} \tag{15}$$

from which it is clear that momentum is conserved for any value of θ:

$$m^i \boldsymbol{v}_0^i + m^j \boldsymbol{v}_0^j = m^i \boldsymbol{v}^i + m^j \boldsymbol{v}^j \tag{16}$$

Moreover, at the point of impact and for g_0 tending to zero, (3) and (7) give the following relation between the velocities:

$$\left(\boldsymbol{n}_0^{ij}\right)^\top (\boldsymbol{v}^i - \boldsymbol{v}^j) = -\frac{1-\theta}{\theta}\left(\boldsymbol{n}_0^{ij}\right)^\top \left(\boldsymbol{v}_0^i - \boldsymbol{v}_0^j\right) \tag{17}$$

from which we identify the restitution coefficient as

$$e = \frac{1-\theta}{\theta} \tag{18}$$

We note that the range of physically acceptable values of e, namely $0 \leqslant e \leqslant 1$ (corresponding to $\tfrac{1}{2} \leqslant \theta \leqslant 1$), implies unconditional stability of the time-stepping scheme.

2.8. Potential contact specification

In the present fully implicit scheme, the potential contacts need to be specified at the beginning of each time step. This may be done in a number of ways based on the current positions and possibly an estimate of the new positions. In the present implementation, the potential contacts are identified as the edges in a Delaunay triangulation where the vertices coincide with the particle centers (see Fig. 2). This definition of potential contacts is usually conservative in the sense that the actual number of contacts may be somewhat lower than the number of potential contacts. On the other hand, the scheme also occasionally leads to particle penetration if a potential contact has not been recorded for two particles that eventually collide. However, this error is very minor and can be reduced, or eliminated entirely, by adjusting the time step. Moreover, if particle penetration does occur in one time step, it will most likely be corrected in the following step. In practice, we observe that this self-correction leads to a scheme that remains stable unless extreme and obviously unreasonable time steps are used.

3. Frictional contact

We now consider the extension to frictional contact. This introduces shear forces acting perpendicular to the normal contact
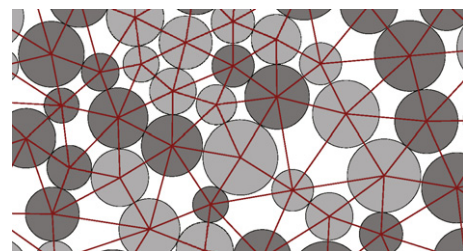

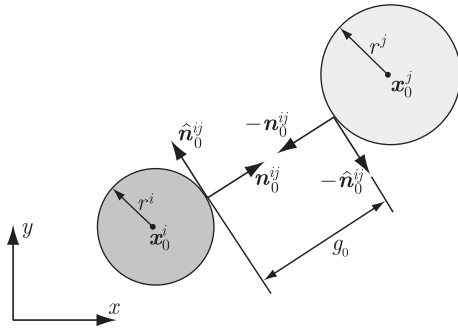**Fig. 2.** Potential contacts as given by Delaunay triangulation.

Fig. 3. Frictional contact geometry.

forces. These shear forces, the magnitude of which is limited by a Coulomb type law, give rise to moments that tend to induce rolling of the particles.

3.1. Sliding friction

Consider first the case where rolling is explicitly precluded. The mixed force–displacement problem (12) can here be extended to include shear forces:

$$\min_{\mathbf{x}} \max_{\mathbf{p},\mathbf{q}} \quad \{\tfrac{1}{2}\Delta\mathbf{x}^\mathsf{T}\overline{\mathbf{M}}\Delta\mathbf{x} - \Delta\mathbf{x}^\mathsf{T}\bar{\mathbf{f}}_0\}$$
$$+\{\Delta\mathbf{x}^\mathsf{T}(\mathbf{N}_0\mathbf{p} + \widehat{\mathbf{N}}_0\mathbf{q}) - \mathbf{g}_0^\mathsf{T}\mathbf{p}\} \tag{19}$$
$$\text{subject to} \quad |\mathbf{q}| - \mu\mathbf{p} \leqslant \mathbf{0}$$

The matrix $\widehat{\mathbf{N}}$ is of the same form as $\mathbf{N}$ but contains entries $\hat{\mathbf{n}} = (-n_y, n_x)^\mathsf{T}$, see Fig. 3 and note that q is taken to be positive opposite to $\hat{\mathbf{n}}$ similar to the sign conventions for p and $\mathbf{n}$. Note also that the above problem is meaningful only for $\mu > 0$ – to recover the frictionless problem it is necessary to again impose $\mathbf{p} \geqslant \mathbf{0}$. The first term in the objective function of (19) is identical to that of (12) while the second term is recognized as a particular form of the principle of maximum plastic dissipation as it applies to the current problem of time discrete frictional contact dynamics. Generally, in the context of frictional problems, the principle of maximum plastic dissipation is problematic in that it predicts a dilation proportional to the friction coefficient while, for real materials, the dilation is significantly smaller and often zero. However, for the present application of time discrete contact dynamics, this issue is much less pronounced and the dilation that does take place can be regarded as an artifact of the time discretization that eventually will be eliminated in the limit of the time step tending to zero. This rather surprising property, which has previously been noted and utilized by Anitescu, Tasora and their co-workers [3,5,45,63–65], is explored in more detail below.

3.2. Consequences of associated sliding rule

The kinematics associated with (19) are recovered by solving the max part of the problem which leads to the following set of optimality conditions:

$$\Delta\mathbf{u}_N = \mathbf{N}_0^\mathsf{T}\Delta\mathbf{x} = -\mu\boldsymbol{\lambda} + \mathbf{g}_0$$
$$\Delta\mathbf{u}_T = \widehat{\mathbf{N}}_0^\mathsf{T}\Delta\mathbf{x} = \text{Sgn}(\mathbf{q})\boldsymbol{\lambda} \tag{20}$$

where subscripts N and T denote the normal and tangential directions and $\lambda \geqslant \mathbf{0}$ are Lagrange multipliers such that $\lambda^I(|q^I| - \mu p^I) = 0$, $I \in \mathcal{C}$, where $\mathcal{C}$ is the set of potential contacts. The important point regarding the above kinematic equations is that the gap, $\mathbf{g}_0$, in time discrete processes tends to cancel the dilation and in such a way that is entirely eliminated in the limit of the time step tending to zero (except in certain pathological cases discussed later on). This
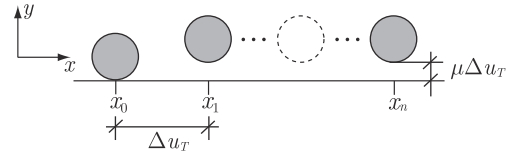

Fig. 4. Quasi-static sliding along a rigid frictional surface.

can be illustrated by the simple example shown in Fig. 4. We here consider a single particle on a rigid frictional surface. The particle is initially at rest on the surface at $(x_0, y_0) = (x_0, 0)$. As such, the gap between the particle and the surface is $g_0 = 0$. A series of tangential displacements $\Delta u_T = \Delta u_x$ of equal size are then imposed in a quasi-static manner. With the application of the first increment, the normal displacement is $-\Delta u_{N,1} = \Delta u_{y,1} = \mu\Delta u_T$ which brings the particle to position $(x_1, y_1) = (x_0 + \Delta u_T, \mu\Delta u_T)$. To continue the time stepping, the new gap is calculated as $g_1 = \mu\Delta u_T$. From (20) the new normal displacement then follows as $\Delta u_{N,2} = g_1 - \mu\Delta u_T = 0$. In other words, no further dilation occurs and the particle slides parallel to the surface at a distance $\mu\Delta u_T$ above it such that an artificial dilation layer – which can be made arbitrarily thin – separates the particle from the surface. Despite this physical separation, contact forces still exist and the behavior of the particle is in every way equal to what it would be with a gap identically equal to zero. To study the more general dynamic case, we consider a particle as shown in Fig. 5. The particle is initially at a distance g_0 from the rigid frictional surface located at $y = 0$ and has an initial horizontal velocity v_T. It is assumed that the particle is within the zone of contact, i.e. within the dilation layer introduced above. This will possibly bring about a further dilation such that the gap increases or the particle may slide along the initial dilation layer as in the quasi-static case. The time discrete governing equations (for $\theta = 1$) are given by:

$$m\Delta u_x = -q\Delta t^2 + mv_T\Delta t$$
$$m\Delta u_y = p\Delta t^2$$
$$q = \mu p \tag{21}$$
$$\Delta u_y = \mu\lambda - g_0$$
$$\Delta u_x = \lambda$$

From these equations, the vertical displacement is found to be

$$\Delta u_y = \frac{\mu v_T\Delta t - g_0}{1 + \mu^2} \tag{22}$$

This solution leads us to define a critical time step:

$$\Delta t_{\text{cr}} = \frac{g_0}{\mu v_T} \tag{23}$$

such that the initial gap will not grow any further for $\Delta t \leqslant \Delta t_{\text{cr}}$ while it will increase for $\Delta t > \Delta t_{\text{cr}}$. In other words, for a finite initial gap, a time step can always be chosen to produce a non-dilative
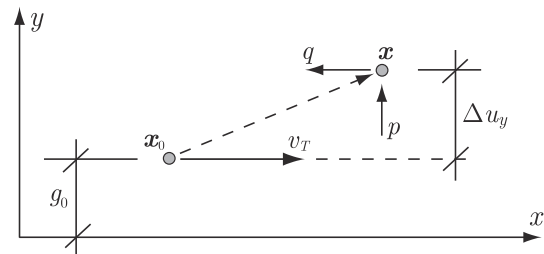

Fig. 5. Dynamic sliding along a rigid frictional surface.

response. This property breaks down for an initial gap identically equal to zero. In this case, the response will be dilative, regardless of the time step. However, in practice, the effects of this possible dilation are in most cases very limited and the slight error possibly made appears to be a small price to pay for maintaining a standard convex variational formulation. Nevertheless, in Section 4, an alternative, nonassociated, formulation is presented along with a newly developed algorithm for linear complementarity problems.

3.3. Including rolling

Angular momentum balance for a particle, i, is given by:

$$J^i \omega^i = r^i \sum_{I \in \mathcal{C}^i} q^I \tag{24}$$

where ω^i is the angular velocity (positive clockwise), J^i is the mass moment of inertia, and $\mathcal{C}^i$ is the set of potential contacts associated with particle i. This equation is extended to the entire system as:

$$J\dot{\omega} = Rq \tag{25}$$

where $\omega = (\omega^1, \ldots, \omega^n)^\top$, $J = \text{diag}(J^1, \ldots, J^n)$, and $R_{il} = r^i$, $I \in \mathcal{C}^i$.

The angular momentum balance equations are discretized in time following the linear momentum balance equations. We thus have

$$\bar{J}\Delta\alpha = R_0 q + \bar{m}_0$$
$$\omega = \frac{1}{\theta}\left[\frac{\Delta\alpha}{\Delta t} - (1 - \theta)\omega_0\right] \tag{26}$$

where α are the angles of rotation and

$$\bar{J} = \frac{1}{\theta \Delta t^2}J, \quad \bar{m}_0 = \bar{J}\omega_0\Delta t \tag{27}$$

The first equation of (26) is readily included in the mixed force–displacement problem (19) to yield

$$\min_{x,\alpha} \max_{p,q} \quad \left\{\frac{1}{2}\Delta x^\top \overline{M}\Delta x - \Delta x^\top \bar{f}_0\right\}$$
$$+\left\{\frac{1}{2}\Delta\alpha^\top \bar{J}\Delta\alpha - \Delta\alpha^\top \bar{m}_0\right\}$$
$$+\left\{\Delta x^\top (N_0 p + \widehat{N}_0 q) - g_0^\top p - \Delta\alpha^\top R_0 q\right\} \tag{28}$$
$$\text{subject to} \quad |q| - \mu p \leqslant 0$$

3.4. Optimality conditions

Following the procedure in Appendix A, the KKT conditions associated with (28) can be shown to comprise the following sets of governing equations pertaining to linear momentum balance:

$$\overline{M}\Delta x + N_0 p + \widehat{N}_0 q = \bar{f}_0, \tag{29}$$

angular momentum balance:

$$\bar{J}\Delta\alpha - R_0 q = \bar{m}_0 \tag{30}$$

sliding friction conditions:

$$|q| - \mu p + s = 0, s \geqslant 0$$
$$\text{diag}(s)\lambda = 0, \lambda \geqslant 0, \tag{31}$$

and kinematics:

$$N_0^\top \Delta x + \mu\lambda - g_0 = 0$$
$$\widehat{N}_0^\top \Delta x - R_0^\top \Delta\alpha - \text{Sgn}(q)\lambda = 0. \tag{32}$$

Regarding the kinematics, we note that the inclusion of rolling further limits dilation in the sense that tangential motion can be accommodated not only by sliding ($\lambda > 0$), but also by rolling ($|\Delta\alpha| > 0$). This lends further credence to the approach of using

an associated sliding rule. Indeed, in the quasi-static deformation of granular materials, such as in triaxial tests, it has long been recognized that sliding occurs only at a small fraction of the contacts [20]. This manifests itself, for example, by the macroscopic friction coefficient being relatively insensitive to the grain scale friction coefficient.

3.5. Displacement based problem

In analogy with the frictionless case, it is readily shown that the mixed force–displacement problem (28) is equivalent to the following displacement based problem:

$$\text{minimize} \quad \frac{1}{2}\Delta x^\top \overline{M}\Delta x + \frac{1}{2}\Delta\alpha^\top \bar{J}\Delta\alpha - \bar{f}_0^\top \Delta x - \bar{m}_0^\top \Delta\alpha$$
$$\text{subject to} \quad \Delta u_N = N_0^\top \Delta x$$
$$\Delta u_T = \widehat{N}_0^\top \Delta x - R_0^\top \Delta\alpha \tag{33}$$
$$|\Delta u_T \leqslant \frac{1}{\mu}\,(g_0 - \Delta u_N)$$

The forces p and q are here recovered as the Lagrange multipliers associated with the first and second set of constraints.

3.6. Force based problem

Alternatively, it is possible to cast (28) and (33) in terms of the following force based problem:

$$\text{maximize} \quad -\frac{1}{2}r^\top \overline{M}^{-1}r - \frac{1}{2}t^\top \bar{J}^{-1}t - g_0^\top p$$
$$\text{subject to} \quad r + N_0 p + \widehat{N}_0 q = \bar{f}_0$$
$$t - R_0 q = \bar{m}_0 \tag{34}$$
$$|q| - \mu p \leqslant 0$$

This problems is somewhat easier to generalize to three dimensions as well as to more complex particle friction laws than that of Coulomb. In our present numerical implementation, this is the problem actually solved. The kinematic variables follow as the Lagrange multipliers associated with the various constraints (Δx with the first set of constraints, $\Delta\alpha$ with the second, and λ with the third) and are computed as part of the solution (see Appendix A).

3.7. Static limit

Omitting the dynamic forces r and t from the problem (34) gives rise to the following static problem which is valid in the limit of Δt tending to infinity:

$$\text{maximize} \quad -g_0^\top p$$
$$\text{subject to} \quad N_0 p + \widehat{N}_0 q = f_{\text{ext}}$$
$$R_0 q = 0 \tag{35}$$
$$|q| - \mu p \leqslant 0$$

It is worth noting the similarity of this problem to those that appear from finite element discretizations of the extremum theorems of classical plasticity, i.e. computational limit analysis [10,23,27,28,70]. The above principle is useful for quasi-static problems governed by an internal pseudo-time rather than physical time. Examples include common soil mechanics laboratory tests such as triaxial tests, quasi-static soil-structure interaction problems such as cone penetration, and various applications in the earth sciences where the time scales are such that the deformations are of a quasi-static nature, for example [17–19,54,55].

3.8. Solution via second-order cone programming

Both the static and dynamic problems, (34) and (35) respectively, can be cast as second-order cone programs (SOCPs). In the

last decade or so a number of very efficient and robust algorithms have been developed for such programs. Of particular note are the codes MOSEK and [2] and SeDuMi [61], both of which are based on a homogeneous interior-point method. We have recently developed an independent code, SONIC, along the same lines as MOSEK and SeDuMi. Though originally designed with continuum plasticity applications in mind [25], it is ideally suited for the kinds of programs generated by the present granular contact dynamics scheme.

A noteworthy feature of SOCP is the straightforward handling of yield surface singularities of the type encountered in the Coulomb friction cone. This is in contrast to most general convex programming solvers which assume (implicitly or explicitly) that the inequality constraints are smooth. Most SOCP solvers, including SONIC, operate with a standard form given by

$$\begin{aligned} \text{minimize} \quad & \boldsymbol{c}^\mathsf{T}\boldsymbol{x} \\ \text{subject to} \quad & \boldsymbol{A}\boldsymbol{x} = \boldsymbol{b} \\ & \boldsymbol{x}_j \in \mathcal{K}_j, \quad j = 1, \dots, n \end{aligned} \tag{36}$$

where it is assumed that the variable vector $\boldsymbol{x}$ can be decomposed into n subvectors such that $\boldsymbol{x} = (\boldsymbol{x}_1, \dots, \boldsymbol{x}_n)^\mathsf{T}$. Each subvector here contains elements $x_1, \dots, x_m$, with m potentially being different for each subvector. For each subvector a single conic constraint is imposed. The two most common forms of conic constraints involve the quadratic cone:

$$\mathcal{K}_q : x_1 \geqslant \sqrt{x_2^2 + \dots + x_m^2}, \tag{37}$$

and the rotated quadratic cone:

$$\mathcal{K}_r : 2x_1 x_2 \geqslant x_3^2 + \dots + x_m^2, x_1, x_2 \geqslant 0, \tag{38}$$

both of which have proved to be very useful in optimization based computational plasticity schemes [25,27].

While the static problem (35) is easily cast in terms of the standard form (36), the dynamic problem (34) requires that the quadratic objective function be transformed into a combination of a linear objective function and a set of rotated quadratic cones [25,27].

4. Linear complementarity scheme

We now consider the modification of the kinematic relations (32) to accommodate an arbitrary dilation. This involves modifying the normal displacement relation to

$$\boldsymbol{N}_0^\mathsf{T}\Delta\boldsymbol{x} + v\lambda - \boldsymbol{g}_0 = \boldsymbol{0} \tag{39}$$

where v is the dilation coefficient. Otherwise, all other governing Eqs. (29)–(32) remain the same. For $v = 0$, the governing equations define what is usually referred to as a frictional contact problem. In the two-dimensional case, it has long been recognized that such problems define a linear complementarity problem (LCP) [1,4,8,34,47,60,66]. While small instances of LCPs often can be solved efficiently by means of pivot based algorithms such as that of Lemke [33], methods for larger problems still lack far behind current SOCP solvers as far as efficiency and robustness is concerned. Alternatively, Newton based algorithms for LCP have also been developed [9] and although these methods in principle offer the same advantages as their convex programming counterparts, their performance has been shown to be highly problem dependent and convergence is generally not guaranteed. Moreover, while convex programs such as SOCPs admit a straightforward analysis of existence and uniqueness properties (and most implementations automatically detect infeasibility, i.e. non-existence), LCPs are in general much harder to gauge with respect to these properties. This leads to a situation where one is unable to distinguish between

algorithmic failure and non-existence of solutions. Regarding the latter possibility – that some problems apparently have no solution even though the physical setup very much would suggest the opposite – has long been recognized as a possibility. A famous example is the paradox of Painlevé who demonstrated non-existence of solutions for a simple frictional contact problem. Although this particular paradox has been resolved [59], its key message, namely that solutions sometimes do not exist, finds abundant support in numerical experiments where solutions often are inexplicably difficult to compute. We note that a similar situation exists in continuum plasticity [12,13,24,35,39].

In the following, an algorithm for the linear complementarity problem relevant to two-dimensional granular contact dynamics is developed. This algorithm is essentially a straightforward modification of the infeasible primal–dual interior-point method used extensively in linear and convex nonlinear programming [11,43,67,68].

4.1. Governing equations

Assuming associated sliding, $\mu = v$, (34) can be written in terms of the quadratic program (QP)

$$\begin{aligned} \text{minimize} \quad & \tfrac{1}{2}\boldsymbol{\sigma}^\mathsf{T}\boldsymbol{C}\boldsymbol{\sigma} + \boldsymbol{g}^\mathsf{T}\boldsymbol{\sigma} \\ \text{subject to} \quad & \boldsymbol{B}^\mathsf{T}\boldsymbol{\sigma} = \boldsymbol{f} \\ & \boldsymbol{F}^\mathsf{T}\boldsymbol{\sigma} \leqslant \boldsymbol{0} \end{aligned} \tag{40}$$

where $\boldsymbol{\sigma} = (\boldsymbol{r}, \boldsymbol{t}, \boldsymbol{p}, \boldsymbol{q})^\mathsf{T}$ and

$$\boldsymbol{C} = \text{diag}[\overline{\boldsymbol{M}}^{-1}, \overline{\boldsymbol{J}}^{-1}, \boldsymbol{0}, \boldsymbol{0}], \ \boldsymbol{g} = (\boldsymbol{0}, \boldsymbol{0}, \boldsymbol{g}_0, \boldsymbol{0})^\mathsf{T}, \tag{41}$$

$$\boldsymbol{B}^\mathsf{T} = \begin{bmatrix} \boldsymbol{I} & \boldsymbol{0} & \boldsymbol{N}_0 & \widehat{\boldsymbol{N}}_0 \\ \boldsymbol{0} & \boldsymbol{I} & \boldsymbol{0} & -\boldsymbol{R}_0 \end{bmatrix}, \boldsymbol{f} = \begin{pmatrix} \boldsymbol{f} \\ \boldsymbol{0} \end{pmatrix}, \tag{42}$$

$$\boldsymbol{F}^\mathsf{T} = \begin{bmatrix} \boldsymbol{0} & \boldsymbol{0} & -\mu\boldsymbol{I} & \boldsymbol{I} \\ \boldsymbol{0} & \boldsymbol{0} & -\mu\boldsymbol{I} & -\boldsymbol{I} \end{bmatrix}, \tag{43}$$

with $\boldsymbol{I}$ being the unit matrix.

The KKT conditions associated with (40) are given by

$$\begin{aligned} \boldsymbol{r}_P &= \boldsymbol{C}\boldsymbol{\sigma} + \boldsymbol{B}\boldsymbol{u} + \boldsymbol{F}\lambda + \boldsymbol{g} = \boldsymbol{0} \\ \boldsymbol{r}_D &= \boldsymbol{B}^\mathsf{T}\boldsymbol{\sigma} - \boldsymbol{f} = \boldsymbol{0} \\ \boldsymbol{r}_F &= \boldsymbol{F}^\mathsf{T}\boldsymbol{\sigma} + \boldsymbol{s} = \boldsymbol{0} \\ \boldsymbol{r}_C &= \boldsymbol{S}\lambda = \boldsymbol{0} \\ \boldsymbol{s}, \lambda &\geqslant \boldsymbol{0} \end{aligned} \tag{44}$$

where superscripts P, D, F, and C denote the primal, dual, frictional sliding, and complementarity residuals respectively, $\boldsymbol{S} = \text{diag}\,(\boldsymbol{s})$, and $\boldsymbol{u}$ and λ are Lagrange multipliers.

For frictional contact with $v < \mu$, only the primal residual requires modification to

$$\tilde{\boldsymbol{r}}_P = \boldsymbol{C}\boldsymbol{\sigma} + \boldsymbol{B}\boldsymbol{u} + \boldsymbol{G}\lambda + \boldsymbol{g} = \boldsymbol{0} \tag{45}$$

where

$$\boldsymbol{G}^\mathsf{T} = \begin{bmatrix} \boldsymbol{0} & \boldsymbol{0} & -v\boldsymbol{I} & \boldsymbol{I} \\ \boldsymbol{0} & \boldsymbol{0} & -v\boldsymbol{I} & -\boldsymbol{I} \end{bmatrix}, \tag{46}$$

Otherwise, all other governing equations are identical in the two cases. These equations define an LCP that can easily be transformed into one of the more common standard forms [14].

4.2. Primal–dual interior-point method

The main idea behind the primal–dual interior-point method is to solve the KKT system of Eq. (44). For this purpose, Newton's method is used with the following modifications. Firstly, instead

of solving for $\mathbf{r}_C = \mathbf{0}$, we aim to find a solution to the augmented system

$$\mathbf{S}\boldsymbol{\lambda} - \beta\mathbf{e} = \mathbf{0} \tag{47}$$

where $\mathbf{e}$ is a vector of ones and $\beta \geqslant 0$ is a barrier parameter that eventually is reduced to zero as the iterations progress. Secondly, in order to satisfy the non-negativity requirements on $\mathbf{s}$ and $\boldsymbol{\lambda}$, the full Newton step is damped so that these variables remain strictly positive throughout. The algorithm thus comprises the following sequence of steps.

Compute barrier parameter:

$$\beta = \gamma (\mathbf{s}^n)^\top \boldsymbol{\lambda}^n \tag{48}$$

Compute Newton direction:

$$\begin{aligned}
\mathbf{C}\delta\boldsymbol{\sigma} + \mathbf{B}\delta\mathbf{u} + \mathbf{G}\delta\boldsymbol{\lambda} &= -\tilde{\mathbf{r}}_P^n \\
\mathbf{B}^\top \delta\boldsymbol{\sigma} &= -\mathbf{r}_D^n \\
\mathbf{F}^\top \delta\boldsymbol{\sigma} + \delta\mathbf{s} &= -\mathbf{r}_F^n \\
\mathbf{S}^n\delta\boldsymbol{\lambda} + \boldsymbol{\Lambda}^n\delta\mathbf{s} &= -(\mathbf{r}_C^n - \beta\mathbf{e})
\end{aligned} \tag{49}$$

Compute step size:

$$\begin{aligned}
&\text{maximize} \quad \alpha \\
&\text{subject to} \quad \mathbf{s}^n + \alpha\delta\mathbf{s} > 0 \\
&\qquad\qquad\quad \boldsymbol{\lambda}^n + \alpha\delta\boldsymbol{\lambda} > 0
\end{aligned} \tag{50}$$

Update:

$$\begin{aligned}
\boldsymbol{\sigma}^{n+1} &= \boldsymbol{\sigma}^n + \theta\alpha\delta\boldsymbol{\sigma} \\
\mathbf{u}^{n+1} &= \mathbf{u}^n + \theta\alpha\delta\mathbf{u} \\
\mathbf{s}^{n+1} &= \mathbf{s}^n + \theta\alpha\delta\mathbf{s} \\
\boldsymbol{\lambda}^{n+1} &= \boldsymbol{\lambda}^n + \theta\alpha\delta\boldsymbol{\lambda}
\end{aligned} \tag{51}$$

Convergence check:

$$\left\| (\tilde{\mathbf{r}}_P^{n+1}, \mathbf{r}_D^{n+1}, \mathbf{r}_F^{n+1}, \mathbf{r}_C^{n+1}) \right\| < TOL? \tag{52}$$

Regarding the algorithmic parameters, a choice of $TOL \simeq 10^{-6}$, $\theta \simeq 0.9$ and $\gamma \simeq 0.5/p$, where p is the length of $\mathbf{s}$, are usually appropriate.

4.3. Predictor-correction scheme

A common enhancement of the basic method outlined above is the predictor–corrector scheme first proposed by Mehrotra [41] (see also [23,43]). This scheme concerns the complementarity condition. Instead of using Newton's method on the augmented system as above, the predictor–corrector scheme aims to solve

$$(\mathbf{S}^n + \delta\overline{\mathbf{S}})(\boldsymbol{\lambda}^n + \delta\overline{\boldsymbol{\lambda}}) = -(\mathbf{S}^n\boldsymbol{\lambda}^n - \beta\mathbf{e}) \tag{53}$$

This is done in two steps. Firstly, by using a value of the barrier parameter $\beta = 0$ and neglecting the higher-order term $\delta\mathbf{S}\delta\boldsymbol{\lambda}$, i.e. by using a regular Newton linearization with $\beta = 0$. This gives an estimate of $\overline{\mathbf{s}}^{n+1} = \mathbf{s}^n + \alpha\delta\overline{\mathbf{s}}$ and $\overline{\boldsymbol{\lambda}}^{n+1} = \boldsymbol{\lambda}^n + \alpha\delta\overline{\boldsymbol{\lambda}}$ which is used to compute an estimate of the barrier parameter according to $\beta = \gamma(\overline{\mathbf{s}}^{n+1})^\top \overline{\boldsymbol{\lambda}}^{n+1}$. Finally, the actual directions $\delta\mathbf{s}$ and $\delta\boldsymbol{\lambda}$ are computed from

$$\mathbf{S}^n\delta\boldsymbol{\lambda} + \boldsymbol{\Lambda}^n\delta\mathbf{s} + \delta\overline{\mathbf{S}}\delta\overline{\boldsymbol{\lambda}} = -(\mathbf{S}^n\boldsymbol{\lambda}^n - \beta\mathbf{e}) \tag{54}$$

and all variables are updated according to (51). For standard linear and quadratic programs the predictor–corrector scheme usually leads to a substantial reduction in the number of iterations and these gains are even more pronounced in the case of LCP, i.e. with $\mathbf{F} \neq \mathbf{G}$.

4.4. Solution of Newton system

Although the Newton system (49) can be solved directly for all variables simultaneously, significant savings can be achieved by reducing it. Straightforward manipulations lead to the following expression for $\delta\boldsymbol{\sigma}$ and $\delta\mathbf{u}$:

$$\begin{bmatrix} \mathbf{C}^* & \mathbf{B} \\ \mathbf{B}^\top & \mathbf{0} \end{bmatrix}^n \begin{pmatrix} \delta\boldsymbol{\sigma} \\ \delta\mathbf{u} \end{pmatrix} = -\begin{pmatrix} \mathbf{r}_P^* \\ \mathbf{r}_D \end{pmatrix}^n \tag{55}$$

where

$$\begin{aligned}
\mathbf{C}^* &= [\mathbf{C} + \mathbf{G}\mathbf{S}^{-1}\boldsymbol{\Lambda}\mathbf{F}^\top] \\
\mathbf{r}_P^* &= [\mathbf{r}_P - \mathbf{G}\mathbf{S}^{-1}(\mathbf{r}_C - \boldsymbol{\Lambda}\mathbf{r}_F)]
\end{aligned} \tag{56}$$

This is followed by the computation of the remaining variables:

$$\delta\mathbf{s} = -\mathbf{r}_F^n - \mathbf{F}^\top\delta\boldsymbol{\sigma}, \quad \delta\boldsymbol{\lambda} = -[\mathbf{S}^{-1}(\boldsymbol{\Lambda}\delta\mathbf{s} + \mathbf{r}_C)]^n \tag{57}$$

The system (55) is recognized as a typical saddle-point system very similar to those that result from mixed finite element formulations (where $\mathbf{C}^*$ in plasticity applications would be similar to the inverse of the elastoplastic tangent). In many cases, with reasonable assumptions about the inequality constraints, it is possible to invert $\mathbf{C}^*$ at negligible cost, thus enabling further savings. Finally, we note that $\mathbf{C}^*$ is unsymmetric except in the case where $\mathbf{G} = \mathbf{F}$.

4.5. Remarks on performance

Although the above algorithm is rather simple its performance in the standard QP case ($\mathbf{G} = \mathbf{F}$) is very good with iteration counts usually in the 20s to low 30s independent of the system size. However, in the general case with $\mathbf{G} \neq \mathbf{F}$, the performance deteriorates markedly, especially for larger systems (more than a few thousand particles) and/or large differences between $\mathbf{F}$ and $\mathbf{G}$, i.e. between the friction and dilation angles, μ and v. Typically, while it for $v = \mu$ is possible to achieve arbitrarily small residuals (subject to problems with ill-conditioning), the performance for $v < \mu$ is often characterized by the progress stalling, usually after 40 or so iterations. This behavior appears to be quite random and is difficult to trace to any particular cause. On the other hand, even with this less than desirable performance, it is in many cases possible to obtain useful solutions as will be demonstrated in the following section.
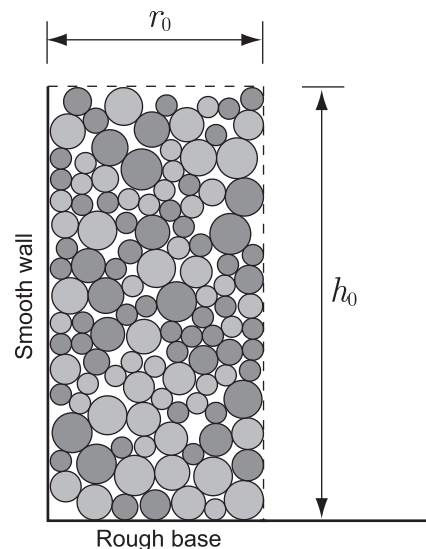

Fig. 6. Granular column setup. Actual columns (Figs. 7 and 8) contain approximately 1500 particles.

5. Examples

In the following, two examples demonstrating the capabilities of the methods developed are presented.

5.1. Collapse of granular column

The first example concerns the collapse of a granular column. The setup is as shown in Fig. 6. At time $t = 0$ a two-dimensional
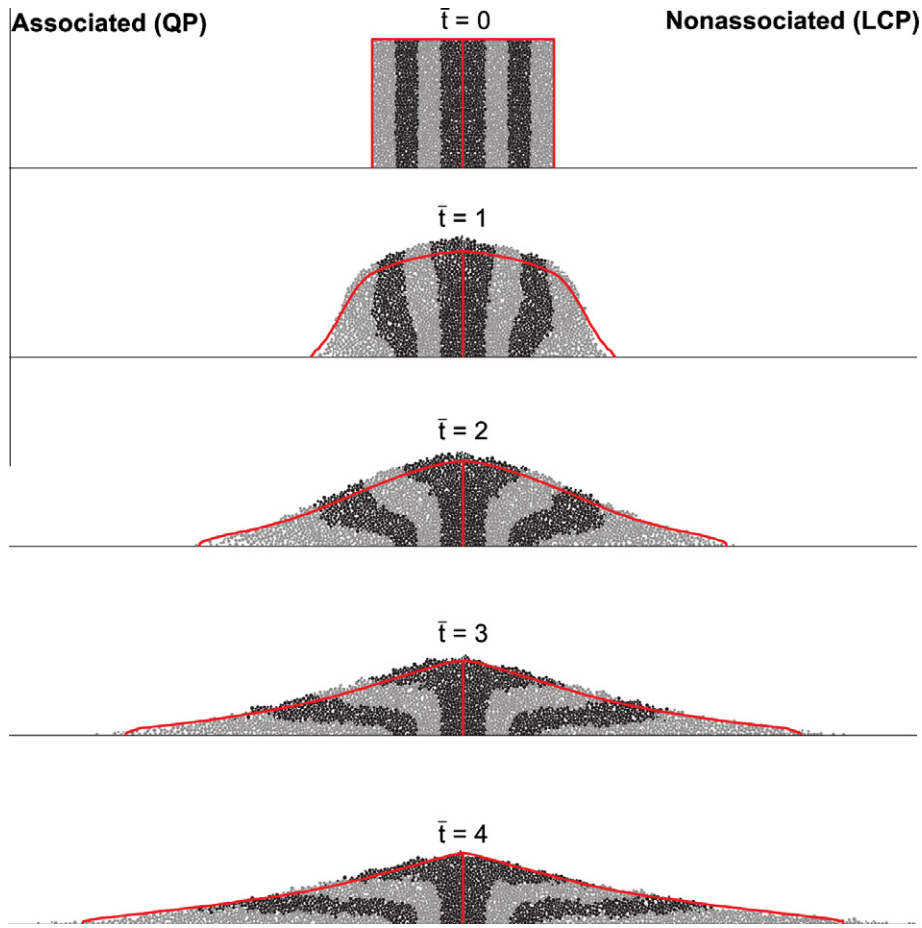

Fig. 7. Collapse of granular column ($\Delta\bar{t} = \Delta t/\sqrt{h_0/g} = 0.04$, $a = h_0/r_0 = 1.42$, $\mu = 0.5$, $v = 0.01$).
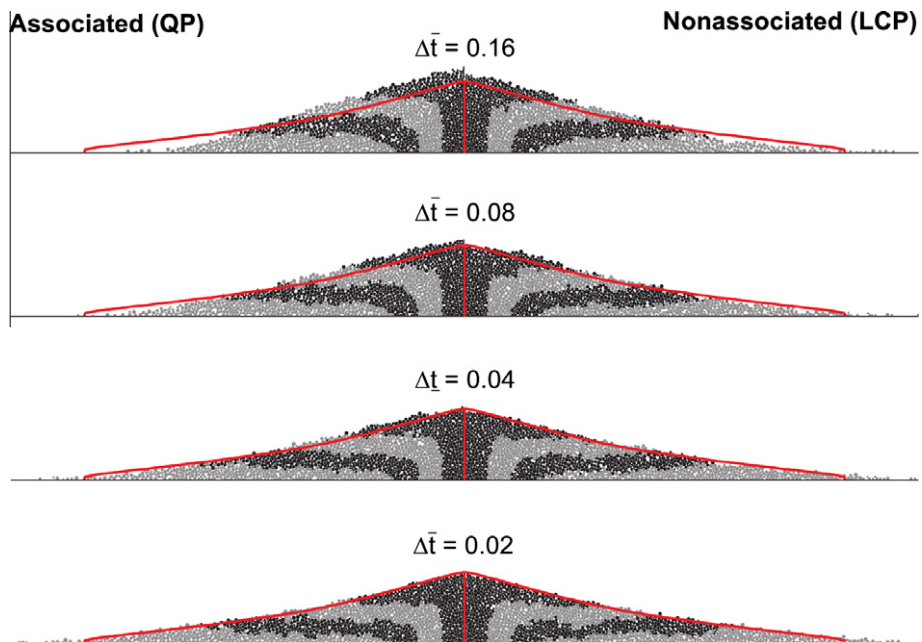

Fig. 8. Granular column at $\bar{t} = t/\sqrt{h_0/g} = 4.0$ ($a = h_0/r_0 = 1.42$, $\mu = 0.5$, $v = 0.01$).
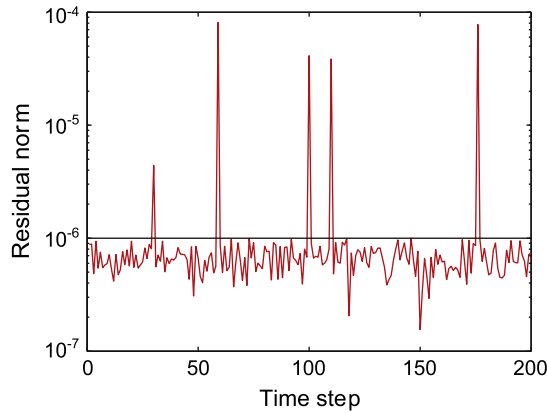
Fig. 9. Granular column problem: residuals of LCP algorithm after 50 iterations with a convergence tolerance of 10^{-6}.
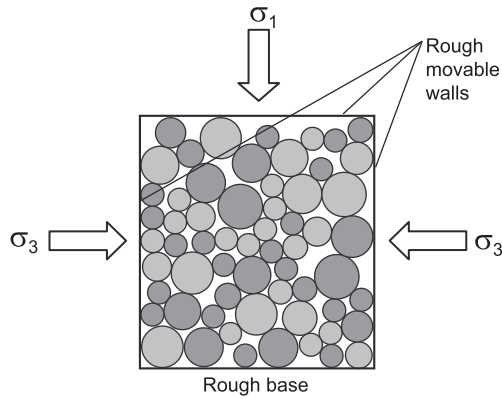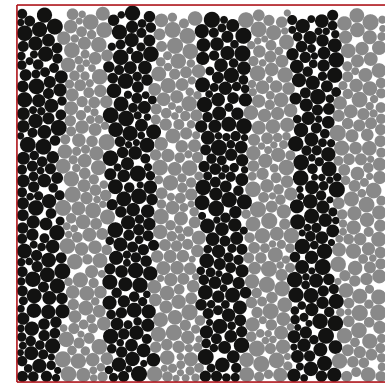

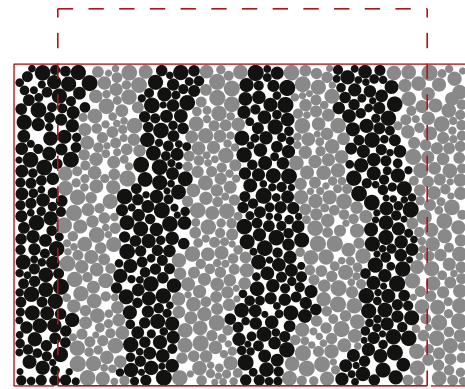**Fig. 10.** Biaxial test setup. Actual samples contain approximately 1000 (Fig. 12) and 26,000 (Fig. 14) particles.

Fig. 12. Biaxial test: initial configuration and at an axial strain of $\varepsilon_a = 0.15$.

column of granular material of height h_0 and diameter r_0 is released and collapses under the action of gravity. The smooth wall on the left is meant to represent a symmetry boundary and the base has the same friction coefficient as that of the grains.

Granular columns, both axisymmetric and two-dimensional (representing plane strain conditions), have been studied quite extensively since they were first introduced in a series of experiments by Lube et al. [36,37] and Lajeunesse et al. [32]. Both discrete models of the kind covered in this paper [29–31,58,58,69] and continuum models [22,31,38] have been proposed and shown to reproduce many of the features of the physical experiments.

In the following we aim to show the favorable agreement between the associated formulation covered in Section 3 and the nonassociated formulation discussed in Section 4. For this purpose, we consider a column with an initial height-diameter ratio of $h_0/r_0 = 1.42$. Identical assemblies consisting of approximately 1500 grains are used in both formulations. The initial porosity is approximately 0.18 and the particle size distribution is uniform with a max–min diameter ratio of $d_{max}/d_{min} = 2.3$. The friction coefficient is $\mu = 0.5$ and the dilation coefficient, in the nonassociated calculation, is $v = 0.01$ (while it is entirely possible to use a value of $v = 0$, this requires the additional constraint $\boldsymbol{p} \geqslant \boldsymbol{0}$ to be enforced). The simulations are initially carried out for a total time of $\bar{t} = t/\sqrt{h_0/g} = 4.0$ using 100 time steps of equal magnitude $\Delta \bar{t} = 0.04$. The results are shown in Fig. 7. We see that the two
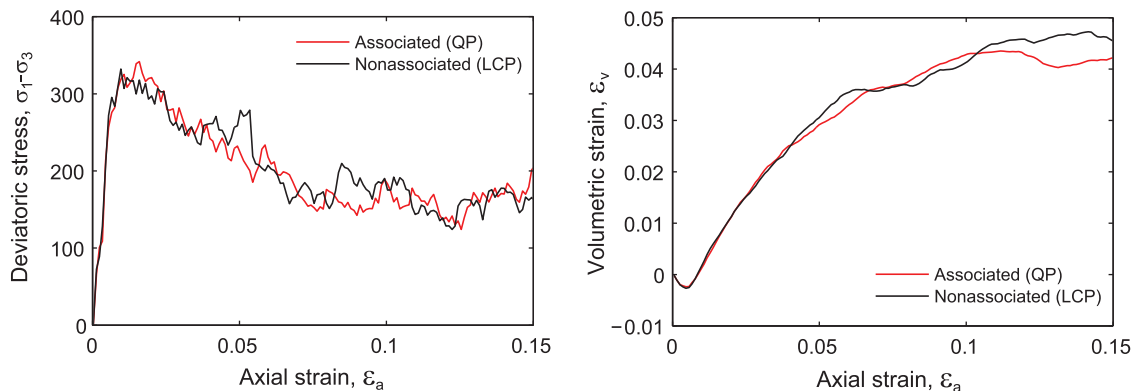

Fig. 11. Biaxial test results for $\mu = \tan 30° \simeq 0.577$ and $v = 0.01$ with a displacement step of $\Delta \varepsilon_a = 0.001$.
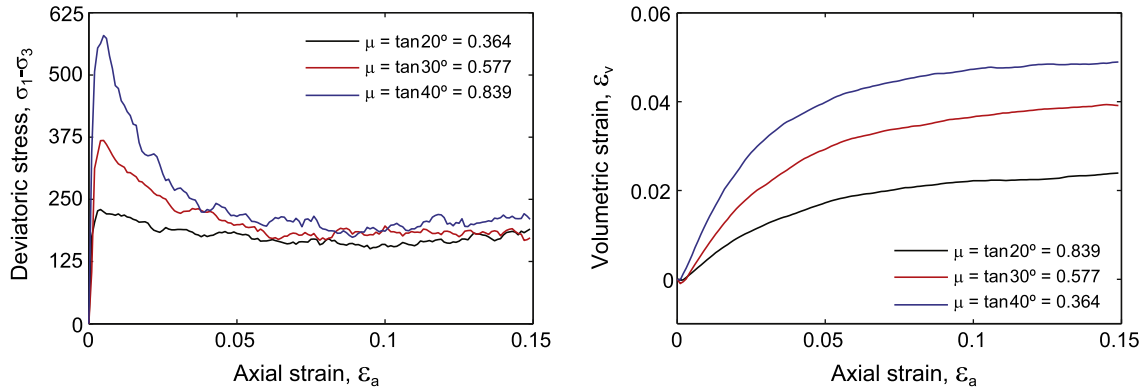
Fig. 13. Biaxial test results for 26,000 particle assemblies. The particle scale frictional sliding rule is associated.

formulations – associated (using QP) and nonassociated (using LCP) – are practically identical. The red lines indicate the results of the continuum formulation of Lagree et al. [31] and show an impressive agreement with the granular contact dynamics results.

Next, we examine the convergence of the two formulations with respect to the final deposit at $\bar{t} = 4.0$. The results for a total of 25, 50, 100 and 200 time steps (corresponding to $\Delta\bar{t} = 0.16$, $0.08, 0.04, 0.02$) are shown in Fig. 8. We here observe a steady convergence as the time step is decreased, with the nonassociated formulation appearing to converge slightly faster. Nevertheless, it can be concluded, for this particular problem, that (*i*) accurate results can be obtained with a relatively coarse time step and (*ii*) the difference between the associated and nonassociated formulations is for all practical purposes negligible.

Regarding the performance of the QP and LCP schemes, the final residuals after a maximum of 50 iterations are shown in Fig. 9 for the simulations with $\Delta\bar{t} = 0.02$. We here see that the LCP algorithm occasionally fails to meet the prescribed convergence threshold, though at the point where progress stalls the residuals are of a magnitude that appears to be acceptable.

5.2. Biaxial test

The second example is a standard biaxial test carried out for a square specimen as shown in Fig. 10. The upper platen is gradually moved downwards while the pressure on the side platens are restricted to a maximum of $\sigma_3 = 125$. Associated with these constraints are Lagrange multipliers that are to be interpreted as the displacements of the side platens. The biaxial test is an example of a problem where the static formulation (35) is appropriate. Again, both associated and nonassociated sliding rules are used.
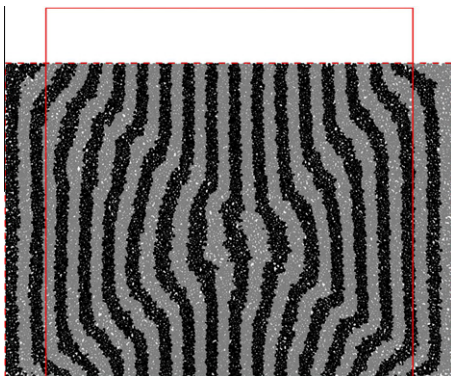

Fig. 14. Biaxial test, $\mu = \tan 30°$: configuration at an axial strain of $\varepsilon_a = 0.15$.

In both cases the friction coefficient is $\mu = \tan 30° \simeq 0.577$ while the dilation coefficient in the latter calculation is $v = 0.01$. The test is initially run using approximately 1000 particles as shown in Fig. 12. The initial porosity is approximately 0.16 and the particle size distribution is uniform with $d_{max}/d_{min} = 2.3$. A total of 150 time steps of equal magnitude are used to impose a total axial strain of $\varepsilon_a = 0.15$.

Assuming that the Coulomb criterion is valid at the macroscopic level, the friction angle is given by:

$$\sin\phi = \frac{\sigma_1 - \sigma_3}{\sigma_1 + \sigma_3} \tag{58}$$

The results shown in Fig. 11 thus correspond to a peak friction angle of approximately 33° while the residual angle is approximately 20°. As in the previous example, we again see a close agreement between the associated and nonassociated solutions. In particular, it is clearly demonstrated that an appreciable grain scale dilation coefficient does not prevent the sample from reaching a critical state. From Fig. 12 we see that the attainment of this critical state has little bearing on the homogeneity of the deformation field, i.e. we do not observe any significant localization of the deformations.

Next, the test is rerun, now with a total of approximately 26,000 particles and the same initial porosity and d_{max}/d_{min} ratio as before. For this test the second-order cone programming solver SONIC was used. The typical solution time per time step was approximately 25 s giving a total solution time for 150 steps of around 1 h. The results for different grain scale friction coefficients are shown in Fig. 13. Due to the larger number of particles, the stress–strain curves are here somewhat more smooth than in the previous example. As expected, the peak strength at low levels of strain becomes more pronounced as the grain scale friction coefficient is increased, while the final residual, or critical state, strength is relatively insensitive to that parameter. Similarly, all samples initially dilate to eventually reach a state where no further volume changes take place. In contrast to the previous example, we now observe (Fig. 14) a distinctly localized pattern of deformations at the critical state which must be attributed to the larger number of particles in the simulation.

6. Conclusions

A series of concise mathematical programming formulations of granular contact dynamics have been developed, implemented and tested. In contrast to traditional discrete element analysis, the present granular contact dynamics formulation uses an implicit time discretization, thus allowing for large time steps. Moreover, in the limit of an infinite time step, the general dynamic formulation reduces to a static formulation that is useful in simulating

common quasi-static problems such as triaxial tests and similar laboratory experiments. It has been shown, through simple toy examples as well as via problems involving thousands of grains, that an associated sliding rule in many practical situations is acceptable and that the dilation that may occur essentially can be viewed as an artifact of the time discretization. Besides a standard quadratic programming solver, a new interior-point algorithm for general linear complementarity problems has been developed and although the performance of this algorithm is less favorable than that of the QP solver, there appears to be some room for improvement, for example via self-dual embedding techniques as commonly used in interior-point methods for convex programming. The essential point, however, is that the use of an associated frictional sliding rule – which allows for the use of QP – appears to be acceptable for typical static and dynamic granular deformation problems such as the ones presented.

Appendix A. Optimality conditions for convex programs

We consider the convex program representing the displacement based form of the frictionless contact problem:

$$
\begin{aligned}
\text{minimize} \quad & \tfrac{1}{2}\Delta \boldsymbol{x}^\top \overline{\boldsymbol{M}}\Delta \boldsymbol{x} - \Delta \boldsymbol{x}^\top \bar{\boldsymbol{f}}_0 \\
\text{subject to} \quad & \boldsymbol{N}_0^\top \Delta \boldsymbol{x} - \boldsymbol{g}_0 \leqslant \boldsymbol{0}
\end{aligned}
\tag{59}
$$

The first-order Karush–Kuhn–Tucker (KKT) optimality conditions associated with (13) can be derived using the following procedure [11,26,43,67]. The inequality constraints are first converted into equality constraints by addition of positively restricted slack variables $\boldsymbol{s}$. The objective function is then augmented by a logarithmic barrier function which eliminates the need to make explicit reference to the fact that $\boldsymbol{s} \geqslant \boldsymbol{0}$. The modified, equality constrained, problem is given by:

$$
\begin{aligned}
\text{minimize} \quad & \tfrac{1}{2}\Delta \boldsymbol{x}^\top \overline{\boldsymbol{M}}\Delta \boldsymbol{x} - \Delta \boldsymbol{x}^\top \bar{\boldsymbol{f}}_0 - \beta \sum_{I\in\mathcal{C}} \ln s^I \\
\text{subject to} \quad & \boldsymbol{N}_0^\top \Delta \boldsymbol{x} - \boldsymbol{g}_0 + \boldsymbol{s} = \boldsymbol{0}
\end{aligned}
\tag{60}
$$

where $\beta > 0$ is an arbitrarily small constant. The standard Lagrange multiplier technique then applies, i.e. the solution to (59) is found by requiring stationary of the Lagrangian

$$
L = \frac{1}{2}\Delta \boldsymbol{x}^\top \overline{\boldsymbol{M}}\Delta \boldsymbol{x} - \Delta \boldsymbol{x}^\top \bar{\boldsymbol{f}}_0 - \beta \sum_{I\in\mathcal{C}} \ln s^I + \boldsymbol{p}^\top \left(\boldsymbol{N}_0^\top \Delta \boldsymbol{x} - \boldsymbol{g}_0 + \boldsymbol{s}\right)
\tag{61}
$$

where $\boldsymbol{p}$ are Lagrange multipliers. The stationary conditions are given by:

$$
\begin{aligned}
\frac{\partial L}{\partial \boldsymbol{x}} &= \overline{\boldsymbol{M}}\Delta \boldsymbol{x} - \bar{\boldsymbol{f}}_0 + \boldsymbol{N}_0 \boldsymbol{p} = 0 \\
\frac{\partial L}{\partial \boldsymbol{p}} &= \boldsymbol{N}_0^\top \Delta \boldsymbol{x} + \boldsymbol{s} - \boldsymbol{g}_0 = \boldsymbol{0} \\
\frac{\partial L}{\partial s^I} &= -\frac{\beta}{s^I} + p^I = 0 \Rightarrow s^I p^I = \beta, \quad I \in \mathcal{C}
\end{aligned}
\tag{62}
$$

The first set of equations are here the equations of motion including the contact forces, namely the Lagrange multipliers $\boldsymbol{p}$. The second set of equations are the non-penetration constraints, and the final set of equations ensure (in the limit of $\beta = 0$) that the contact forces are non-negative and positive only if the non-penetration conditions are satisfied with equality.

References

[1] Acary V, Brogliato B. Numerical methods for nonsmooth dynamical systems. Springer; 2008.
[2] Andersen ED, Roos C, Terlaky T. On implementing a primal-dual interior-point method for conic quadratic optimization. Mathe Programm 2003;95:249–77.
[3] Anitescu M. Optimization-based simulation of nonsmooth rigid multibody dynamics. Mathe Program A 2006;105:113–43.
[4] Anitescu M, Potra FA. Formulating dynamic multi-rigid-body contact problems with friction as solvable linear complementarity problems. Nonlin Dynam 1997;14:231–47.
[5] Anitescu M, Hart GD. A constraint-stabilized time-stepping approach for rigid multibody dynamics with joints, contact and friction. Int J Numer Meth Eng 2004;60:2335–71.
[6] Anon. Quadratic programming <http://en.wikipedia.org/wiki/Quadratic_programming>; 2011.
[7] Anon. Second-order cone programming; 2011.
[8] Baraff D. Fast contact force computation for nonpenetrating rigid bodies. Comput Graph 1994;28:23–42.
[9] Billups SC, Dirkse SP, Ferris MC. comparison of large scale mixed complementarity problem solvers. Comput Optimiz Appl 1997;7:3–25.
[10] Borges LA, Zouain N, Huespe AE. A nonlinear optimization procedure for limit analysis. Euro J Mech, A/Solids 1996;15(3):487–512.
[11] Boyd S, Vandenberghe L. Convex optimization. Cambridge University Press; 2006.
[12] Carter JP, Poon MSB, Airey DW. Numerical and semi-analytical techniques for footings subjected to combined loading. In: Proceedings of IACMAG 11. Turin; 2005. p. 163–76.
[13] Clausen J, Krabbenhoft K. Existence and uniqueness of solutions in nonassociated Mohr–Coulomb elastoplasticity. In: Proceedings of WCCM VIII. Venice; 2008.
[14] Cottle RW, Pang JS, Stone RE. The linear complementarity problem. Academic Press; 1992.
[15] Cundall PA, Strack ODL. A discrete numerical model for granular assemblies. Geotechnique 1979;29:47–65.
[16] Donze F, Magnier VRSA. Advances in discrete element method applied to soil, rock and concrete mechanics. Electron J Geotech Eng 2009:1–44.
[17] Donze F, Mora P, Magnier SA. Numerical simulation of faults and shear zones. Geophys J Int 1994;116:46–52.
[18] Egholm DL. A new strategy for discrete element numerical models: 1. Theory. J Geophys Res 2007;112:B05203.
[19] Egholm DL, Sandiford M, Clausen OR, Nielsen SB. A new strategy for discrete element numerical models: 2. Sandbox applications. J Geophys Res 2007;112:B05204.
[20] Estrada N, Azema E, Radjai F, Taboada A. Identification of rolling resistance as a shape parameter in sheared granular media. Phys Rev E 2011;84:011306.
[21] Jean M. The non–smooth contact dynamics method. Comput Meth Appl Mech Eng 1999;177:235–57.
[22] Kerswell RR. Dam break with coulomb friction: a model for granular slumping? Phys Fluids 2005;17:057101.
[23] Krabbenhoft K, Damkilde L. general nonlinear optimization algorithm for lower bound limit analysis. Int J Numer Meth Eng 2003;56:165–84.
[24] Krabbenhoft K, Karim MR, Lyamin AV, Sloan SW. Associated computational plasticity schemes for nonassocited frictional materials. Int J Numer Meth Eng, in press. doi:10.1002/nme.3358.
[25] Krabbenhoft K, Lyamin AV. Computational Cam clay plasticity using second-order cone programming. Comput Meth Appl Mech Eng 2012;209–212:239–49.
[26] Krabbenhoft K, Lyamin AV, Hjiaj M, Sloan SW. A new discontinuous upper bound limit analysis formulation. Int J Numer Meth Eng 2005;63:1069–88.
[27] Krabbenhoft K, Lyamin AV, Sloan SW. Formulation and solution of some plasticity problems as conic programs. Int J Solids Struct 2007;44:1533–49.
[28] Krabbenhoft K, Lyamin AV, Sloan SW. Three-dimensional Mohr–Coulomb limit analysis using semidefinite programming. Commun Numer Meth Eng 2008;24:1107–19.
[29] Lacaze L, Kerswell RR. Axisymmetric granular collapse: a transient 3d flow test of viscoplasticity. Phys Rev Lett 2009;102:108305.
[30] Lacaze L, Phillips JC, Kerswell RR. Planar collapse of a granular column: experiments and discrete element simulations. Phys Fluids 2008;20:063302.
[31] Lagree PY, Staron L, Popinet S. The granular column collapse as a continuum: validity of a two-dimensional Navier–Stokes model with a μ(i)-rheology. J Fluid Mech, in press. doi:10.1017/jfm.2011.335.
[32] Lajeunesse E, Mangeney-Castelneau A, Vilotte JP. Spreading of a granular mass on an horizontal plane. Phys Fluids 2004;16:2381–731.
[33] Lemke CE. Bimatrix equilibrium points and mathematical programming. Manag Sci 1965;11(65):681–9.
[34] Lötstedt. Coulomb friction in two-dimensional rigid body systems. Zeitschrift fnr Angewandte Mathematik und Mechanik 1981;61:605–15.
[35] Loukidis D, Salgado R. Bearing capacity of strip and circular footings in sand using finite elements. Comput Geotech 2009;36:871–9.
[36] Lube G, Sparks HEHRSJ, Freundt A. Collapses of two-dimensional granular columns. Phys Rev E 2005;72:041301.
[37] Lube G, Sparks HEHRSJ, Hallworth MA. Axisymmetric collapses of granular columns. J Fluid Mech 2004;508:175–99.
[38] Mangeney-Castelnau A, Bouchut F, Vilotte JP, Lajeunesse E, Aubertin A, Pirulli M. On the use of saint venant equations to simulate the spreading of a granular mass. J Geophys Res 2005;110:B09103.
[39] Manzari MT, Nour MA. Significance of soil dilatancy in slope stability analysis. J Geotech Geoenviron Eng 2000;126:75–80.
[40] McNamara S, Herrmann H. Measurement of indeterminacy in packings of perfectly rigid disks. Phys Rev E 2004;70:061303.
[41] Mehrotra S. On the implementation of a primal-dual interior point method. SIAM J Optim 1992;2:575–601.

[42] Moreau JJ. Some numerical methods in multibody dynamics: application to granular materials. Euro J Mech A/Solids 1994;13:93–114.

[43] Nash SG, Sofer A. Linear and nonlinear programming. New York, N.Y: McGraw-Hill; 1996.

[44] Nouguier-Lehon C, Cambou B, Vincens E. Influence of particle shape and angularity on the behavior of granular materials: a numerical analysis. Int J Numer Anal Meth Geomech 2003;27:1207–26.

[45] Petraa C, Gavreab B, Anitescu M, Potraa F. A computational study of the use of an optimization-based method for simulating large multibody systems. Optim Meth Softw 2009;24:871–94.

[46] Pfeiffer F, Foerg M, Ulbrich H. Numerical aspects of nonsmooth multibody dynamics. Comput Meth Appl Mech Eng 2006;195:6891–908.

[47] Pfeiffer F, Glocker C. Multibody dynamics with unilateral contacts. Wiley; 1996.

[48] Radjai F, Michel J, Moreau JJ, Roux S. Force distributions in dense two-dimensional granular systems. Phys Rev Lett 1996;77:274–7.

[49] Radjai F, Richefeu V. Contact dynamics as a nonsmooth discrete element method. Mech Mater 2009;41:715–28.

[50] Renouf M, Dubois F, Alart P. Parallel version of the nonsmooth contact dynamics algorithm applied to the simulation of granular media. J Comput Appl Math 2004;168:375–82.

[51] Ries A, Wolf DE, Unger T. Shear zones in granular media: three-dimensional contact dynamics simulation. Phys Rev E 2007;195.

[52] Saussine G, Cholet C, Gautier PE, Dubois F, Bohatier C, Moreau JJ. Modelling ballast behaviour under dynamic loading part 1: a 2D polygonal discrete element method approach. Comput Meth Appl Mech Eng 2006;195:2841–59.

[53] Simo JC, Hughes TJR. Computational inelasticity. Springer-Verlag; 1998.

[54] Souloumiac P, Krabbenhoft K, Leroy YM, Maillot B. Failure in accretionary wedges with the maximum strength theorem: numerical algorithm and 2d validation. Comput Geosci 2010;14:793–811.

[55] Souloumiac P, Leroy YM, Maillot B, Krabbenhoft K. Predicting stress distributions in fold-and-thrust belts and accretionary wedges by optimization. J Geophys Res 2009;114:B09404.

[56] Souza de Neto EA, Peric D, Owen DRJ. Computational methods for plasticity: theory and applications. Elsevier; 2009.

[57] Staron L, Hinch EJ. Study of the collapse of granular columns using two-dimensional discrete-grain simulation. J Fluid Mech 2005;545:1–27.

[58] Staron L, Hinch EJ. The spreading of a granular mass: role of grain properties and initial conditions. Granul Matter 2007;9:205–17.

[59] Stewart DE. Convergence of a time-stepping scheme for rigid-body dynamics and resolution of Painleve's problem. Arch Ration Mech Anal 1998;154:215–60.

[60] Stewart DE. Rigid-body dynamics with friction and impact. SIAM Rev 2000;42:3–39.

[61] Sturm JF. SeDuMi 1.02, a MATLAB toolbox for optimizing over symmetric cones. Optim Meth Softw 1999;11–12:625–53. <http://sedumi.mcmaster.ca/>.

[62] Taboada A, Chang KJ, Radjai F, Bouchette F. Rheology force transmission and shear instabilities in frictional granular media from biaxial numerical test using the contact dynamics method. J Geophys Res 2005;110:1–24.

[63] Tasora A, Anitescu M. A convex complementarity approach for simulating large granular flows. J Comput Nonlin Dynam 2010;5:031004.

[64] Tasora A, Anitescu M. An iterative approach for cone complementarity problems for nonsmooth dynamics. Comput Optim Appl 2010;47:207–35.

[65] Tasora A, Anitescu M. A matrix-free cone complementarity approach for solving large-scale, nonsmooth, rigid body dynamics. Comput Meth Appl Mech Eng 2011;200:439–53.

[66] Tin–Loi F, Xia SH. An iterative complementarity approach for elastoplastic analysis involving frictional contact. Int J Mech Sci 2003;45:197–216.

[67] Vanderbei RJ. Linear programming: foundations and extensions. Springer-Verlag; 2001.

[68] Wright SJ. Primal-dual interior–point methods. Philadelphia: SIAM; 1997.

[69] Zenit R. Computer simulations of the collapse of a granular column. Phys Fluids 2005;17:031703.

[70] Zouain N, Herskovits J, Borges LA, Feijóo RA. An iterative algorithm for limit analysis with nonlinear yield functions. Int J Solids Struct 1993;30(10):1397–417.